Calibration-free laser-induced breakdown spectroscopy

Jörg Hermann

Chapter 1
Calibration-free laser-induced breakdown spectroscopy

Jörg Hermann[1*]

[1] *Laboratoire Lasers, Plasmas et Procédés Photoniques (LP3), Centre National de la Recherche Scientifique, 13288, Marseille, Avenue de Luminy, France*

*jorg.hermann@univ-amu.fr

Abstract: The purpose of this chapter is to give an introductive overview on the so-called *calibration-free* laser-induced breakdown spectroscopy that enables straightforward compositional analysis of materials via modeling of the plasma emission spectrum, without any need of measurement calibration with standard samples. The proposed physical models, their validity conditions, and the experimental requirements are discussed. Based on results reported in literature, a critical review of the analytical performance is given. Finally, the remaining challenges are outlined, and a tentative picture of the perspectives in terms of further improvements and potential applications is drawn.

Keywords: laser-induced breakdown spectroscopy, calibration-free, elemental analysis, plasma modeling, plasma diagnostics, self-absorption

1.1. Introduction

Calibration-free laser-induced breakdown spectroscopy was introduced by Ciucci et al. [1] to overcome difficulties of LIBS measurement quantification due to the so-called *matrix effects*. Matrix effects refer to all phenomena that alter the amplitude of the analytical signal, independently of the analyte concentration. They are particularly severe in LIBS analysis, in which the processes of probe sampling and signal excitation occur in a unique step. Thus, the properties of the laser-generated plasma depend on the laser-induced sample vaporization process, that itself depends on the materials physicochemical properties, including the elemental composition. In analysis via inductively coupled plasma atomic emission spectrometry (ICP-AES), for example, the sample material is transported in form of aerosols within an argon flux into the ICP plasma. The plasma is dominated by the argon buffer gas and the plasma properties are therefore almost independent of the sample material composition.

Beside the need to overcome the difficulties of LIBS analysis due to the matrix effects, calibration-free laser-induced breakdown spectroscopy (CF-LIBS) presents a unique and revolutionary alternative to the traditional analytical techniques based on the calibration with standard samples. Calibration-free analysis open new perspectives in modern world applications, characterized by a strongly increasing need of low-cost, rapid, sensitive, in-situ analyses. That is why CF-LIBS attracted huge interest over the last two decades.

The unique opportunity of performing quantitative measurements of the materials elemental composition without calibration is due to singular properties of the plasma produced by pulsed laser ablation. Indeed, the rapid and localized vaporization of matter generates a small-sized, high-density plasma, characterized by a large degree of ionization. In such a plasma, the rates of collisional

excitation and desexcition largely overcome the rates of radiative decay, a situation that favours the establishment of local thermodynamic equilibrium (LTE) [2]. The LTE state gives straightforward access to accurate plasma modeling via simple statistical laws, and the plasma emission spectrum can be calculated as a function of a few parameters only.

This motivated modeling of laser-induced plasmas in materials processing, where the plasma plays a key role in the processing optimization. Thus, emission spectra of plasmas produced by infrared or ultraviolet laser pulses in different gas atmospheres were compared to the emission predicted by the LTE model, and the temperature was derived from Boltzmann diagrams [3, 4]. Ciucci et al. [1] combined LTE plasma modeling with the assumption of congruent mass transfer from the solid sample towards the plasma to enable direct elemental composition measurements. The method ignored self-absorption and possible nonuniform spatial distributions of temperature and densities, although these effects were shown to alter the emission spectrum of the laser-induced plasma [5].

Unless the limitation of validity to a rather ideal plasma emission source, the CF-LIBS method by Ciucci et al. attracted great interest, and many research groupes applied the method for analysis of various types of materials [6]. The enthusiastic use was promoted by the simplicity of CF-LIBS implementation. Based on the simple recording of measured line intensities in the multielemental Boltzmann diagram, the method was accessible to all research groups having a LIBS system of known apparatus response function. The numerous reported results illustrated rapidly the limitations of the approach. Thus, ammended approaches have been proposed to account for non-stoichiometric mass transfer from the sample to the plasma [7, 8], self-absorption [9, 10], and plasma

non-uniformity [11, 12]. The corrections were however difficult to apply, and therefore ignored in most compositional analyses via calibration-free LIBS.

Methods via the simulation of the plasma emission spectrum have been proposed later [13, 14, 15]. Based on the calculation of the spectral radiance, these approaches account intrinsically for self-absorption. Most of them exploit simple analytical solutions of the radiation transfer equation according to Hermann et al. [5]. The plasma is thus described by one or two uniform plasma zones, representing the hot plasma core and the cold border. The advantage lies in the short calculation time that offers rapid analysis results, when implemented in an appropriate calculation loop.

Given the rather moderate accuracy that was reached in numerous calibration-free LIBS measurements, several recent approaches were ammended by including a calibration step with a single standard sample [16, 17, 18]. These methods aim to compensate errors due to the unprecisely known apparatus response, or the low accuracy of transitions probabilities.

To illustrate the achievements and remaining challenges of calibration-free LIBS, the validity conditions of the physical model and the proposed approaches will be discussed in Sections 1.2 and 1.3, respectively. A critical review of the analytical performance will be given in Section 1.4, before closing this chapter with concluding remarks and an outlook on the perspectives of calibration-free LIBS anaysis.

1.2. Validity conditions of physical model

1.2.1. Congruent mass transfer from solid towards plasma

The question of congruent mass transfer from the solid sample towards the plasma is crucial in calibration-free LIBS analysis. Most aproaches are based on the assumption that the elemental composition of the plasma equals that of the sample material. Only a few authors were calling into question the validity of this assumption, proposing corrections for non-stoichiometric sample vaporization [7, 8].

The congruent character of vaporization is naturally related to the fundamental mechanisms of the laser ablation process. In case of thermal evaporation, when liquid and gaseous phases are in thermodynamic equilibrium, the vaporization pressures of the individual elements differ according to the Clausius-Clapeyron equation, and the liquid and gas phases have unequal elemental compositions. In oppositon, at high rates of vaporization, there is no time for segregation, and all elements are transferred simultaneously from the solid phase into the plasma. This regime, called *phase explosion*, is typically reached during laser irradiation of materials with high intensity.

The question of congruent vaporization is crucial also for other applications of laser ablation. For example, in pulsed laser deposition (PLD), the stoichiometric mass transfer from the laser-irradiated target towards the substrate is desired to deposit a thin film with an elemental composition equal to that of the target material [19]. Non-stoichiometric mass transfer was often reported, but mainly attributed to the expansion dynamics of the vaporized material.

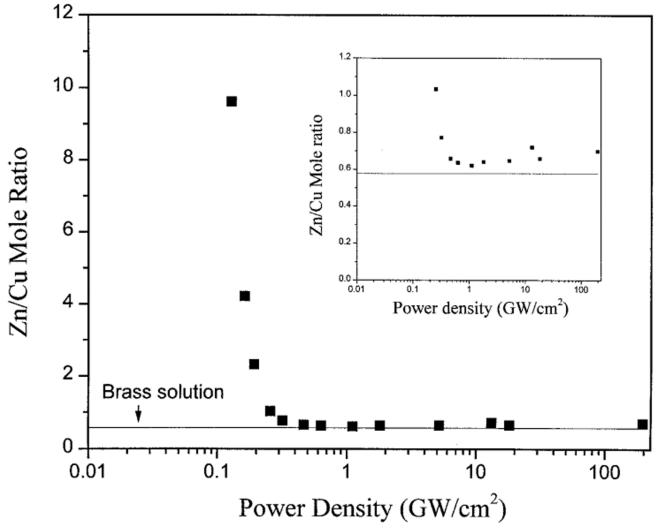

Figure 1.1: Zn/Cu mole ratio vs laser power density measured for brass via laser ablation inductively coupled plasma atomic emission spectroscopy (Adapted from Mao et al. [20]).

Compared to LIBS experiments, pulsed laser deposition is operated with much lower laser fluence, and non-congruent ablation due to thermal evaporation is therefore more probable in PLD.

The influence of laser fluence on the congruent character of laser ablation was investigated by Mao et al. [20] through compositional measurements in laser ablation inductively coupled plasma atomic emission spectroscopy. Measuring the composition of laser-vaporized brass, the authors show that the Zn/Cu mole ratio within the vapor was close to the nominal value of the brass sample, for laser irradiation with a fluence that significantly exceeds the threshold of ablation (see Figure 1.1). When decreasing the laser fluence to values close to the ablation threshold, the zinc content increased, as expected for the case of thermal evaporation, according to the enthalpie of vaporization of zinc much lower than that of copper.

Materials analysis via LIBS are typically operated with high laser fluence, exceeding the threshold of material ablation by more than one or two orders of magnitude. In this regime of laser irradiation, the vaporization process can be safely considered as congruent [21].

1.2.2. Local thermodynamic equilibrium

The state of local thermodynamic equilibrium is established when the rates of collisions are large enough, so that collisional processes of excitation and desexcitation dominate the radiative decay. Due to their high mobility, the electrons govern the collisonal processes, and the establishment of LTE is conditioned by a minimum value of electron density [22]. The equilibrium state implies the principle of microscopic reversibility, each process is thus counterbalanced with the respective inverse process. As the laser-induced ablation plume is characterized by a fast expansion dynamics during which the plasma cools down and recombines, microreversibility can be achieved only if the plasma reaches a quasi-stationary state. In that case, the collisional rates are large enough so that the time of thermalization - that is the time necessary to establish the equilibrium - is small compared to the characteristic times of temperature and electron density changes. An additional condition arises from the spatial distribution of plasma temperature and densities. Equilibrium can be established only if the mean free path between the particle collisions is short compared to the characteristic lengths of temperature and density variations.

Due to the spatio-temporal variation of plasma properties, checking the LTE validity conditions is a challenging task [23]. The LTE state is therefore rarely proven, and most investigations of local thermodynamic equilibrium were lim-

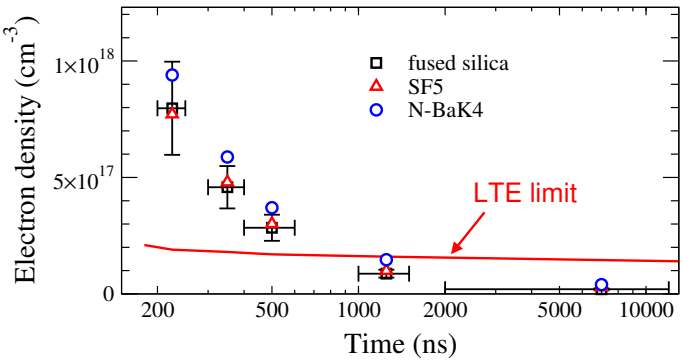

Figure 1.2: Electron density versus measurement time for laser-induced plasmas on optical glasses. The minimum n_e-value required for LTE according to the McWhriter criterion is indicated by the red curve. (Adapted from Gerhard et al. [28])

ited to the comparison of the measured electron density to the minimum value predicted by the McWhirter criterion.

The time of LTE onset was subject of a controverse discussion. Several authors estimated that LTE is established after a time ≥ 1 μs only [24, 25]. Contrarily, other studies indicate that the equilibrium is established in a much shorter time, and also lost rapidly [26, 27]. Performing spectra recordings for various measurement delays, Gerhard et al. [28] showed that accurate calibration-free LIBS analysis of glass is possible for $t \leq 1\mu$s only, when the electron density exceeds the minimum value required for LTE (see Figure 1.2).

Lam et al. [24] investigated the equilibrium state of the plasma generated on Ti-doped sapphire, comparing the electronic excitation temperatures of atoms and ions to the rotational temperature of AlO radicals. The authors found that the rotational temperature was significantly lower than the excitation temperature of the atomic species, and attributed the difference to the failure of equilibrium, ignoring however the possible occurence of a temperature gradient. Indeed, molecular emission was found to originate mostly from the

lower temperature plasma border, whereas atomic emission comes from the hot plasma core mainly [29].

The validity of LTE was also investigated numerically using collisional-radiative modeling [30, 31]. The calculations performed for metals indicate that the equilibrium state is reached rapidly after the laser pulse, and lost after a time that depends on laser pulse energy, and on the surrounding gas atmosphere. Confirmed by numerous experimental investigations, it is now well accepted that LTE is achieved, if the experimental conditions are properly chosen.

Moreover, the LTE validity depends on the elements. This is illustrated by the dependence of the McWhirter criterion on the largest energy gap between electronic states [22]. Thus, atoms with huge energy gaps, such as C, H, N and O, need higher electron density to establish Boltzmann equilibrium distributions than metal atoms with many electronic states, lying close to each others.

1.2.3. Spatial distribution of plasma

Plasmas have always nonuniform spatial distribution as they are surrounded by a cold environment. They are typically composed by a hot core and a cold border. The plasma produced by laser ablation in ambient air, or other gas atmospheres, evolves in both the vapor plume and the gas close to the vapor-gas contact front. In LIBS analysis, only emission from the vaporized sample material is of interest, and the question of plasma uniformity is thus restricted to inner part of the plasma, represented by the vapor plume. It is therefore possible that the plasma volume of interest is characterized by spatially uniform distributions of temperature and densities, although the laser-produced plasma is globally nonuniform.

Spatially resolved spectroscopic observations of plasmas produced by laser ablation under vaccum, or in low pressure atmospheres, show that the most energetic plume species have the fastest expansion velocities [4, 32]. When ablation occurs in ambient gas at atmospheric pressure, the most energetic species are the first to interact with the surrounding backround gas, followed by the lower energetic plume species. Due to cooling via energy exchange with the background gas, the plasma evolutes towards the nominal spatial distribution, characterized by a hot core and a lower temperature border. According to this scenario, it is expected that there exists a time window, during which the vapor plume has a rather uniform spatial distribution. The lifetime of quasi-uniform plume distribution depends on the nature of the background gas. This was illustrated through comparative investigations of plasma diagnostics in air and argon, showing that the plasma produced under inert gas is almost uniform over a duration of the order of a microsecond, whereas the plasma generated in ambient air remains nonuniform for the entire plasma lifetime [33].

The influence of the background gas on plasma uniformity is evidenced by the spectral shape of the resonance line displayed in Figure 1.3 for laser ablation of indium in argon and ambient air. The line profile observed in air exhibits an absorption dip that is attributed to the presence of the low temperature strongly absorbing plasma border. As a result of the reduced vapor-gas energy exchange, the cold absorbing layer is absent for ablation in argon, and the absorption dip is not observed.

Only a few calibration-free LIBS approaches consider plasma nonuniformity [14, 15, 35]. Their application is challenging because of the large number of parameters used to describe the emission from a nonuniform plasma [36]. Moreover, the need of considering the spatial distribution in the calculation

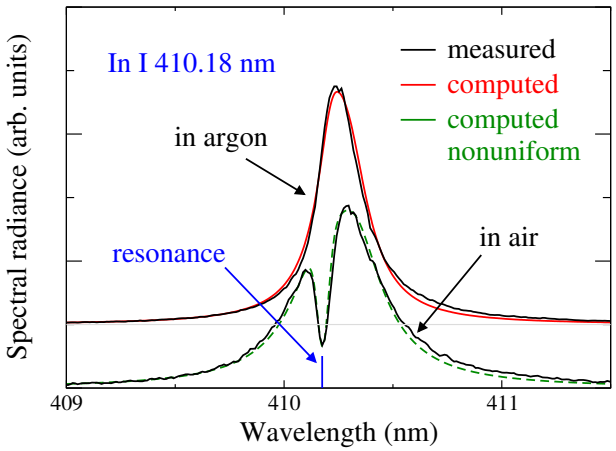

Figure 1.3: Resonance transition observed during laser ablation of pure indium for $t = 500$ ns. The line shapes measured for argon and air are compared to the spectral radiances of uniform and nonuniform LTE plasmas, respectively. (Adapted from Hermann et al. [34]).

of plasma emission was found to be less important for lines of negligible self-absorption [29]. Indeed, the plasma emission originates mostly from the hot core, while the cold border contributes mainly through absorption. The cold border can therefore be often ignored when optically thin lines are considered. When lines of significant self-absorption are measured, the plasma nonuniformity has to be considered, if the plasma is generated in ambient air. The consideration of plasma nonuniformity is also required for elements of very low ionization energy, as their atomic emission from the cold border is significant. For laser irradiation in argon, the plasma emission was shown to be well described by the simple uniform LTE model [34].

1.2.4. Self-absorption

The assumption of negligible self-absorption is made in many calibration-free LIBS measurements [17, 37], often without any evaluation of the optical thickness [38]. In many cases, the assumption is simply justified by the moderate or low elemental fraction. The principal reason of the simplification is that CF-LIBS analysis based on the presentation of measured line intensities in the multi-elemental Boltzmann plot [1] does not give access to the evaluation of the optical thickness. The amount of self-absorption depends on the line profile, and its evaluation is therefore not straightforward [39]. Most of the proposed approaches to evaluate and to correct self-absorption are based on the analytical solution of the radiation transfer equation, assuming a uniform plasma in LTE [5, 9, 10, 40]. They mostly differ in simplifying assumptions of the line profile or computational details. Self-absorption is sometimes presented as an advantage [41, 42], and some authors propose corrections that enable analytical measurements with even strongly self-absorbed lines [43, 44].

Basically, the processes of emission and absorption are correlated. In the case of Boltzmann equilibrium, the most intense lines are generally also the transitions of largest optical thickness. The selection of the appropriate analytical lines is therefore based on a compromise between largest signal-to-noise ratio and lowest optical thickness.

The influence of self-absorption on the analytical performance of LIBS measurements is illustrated by the curves of growth presented in Figure 1.4 for two lines of germanium, having significant different optical thicknesses. Both line-center (a,b) and line-integrated (c,d) intensity measurements are considered. The measured intensities are compared to the spectral radiance computed by considering and ignoring self-absorption using Equations 1.6 and 1.7, respec-

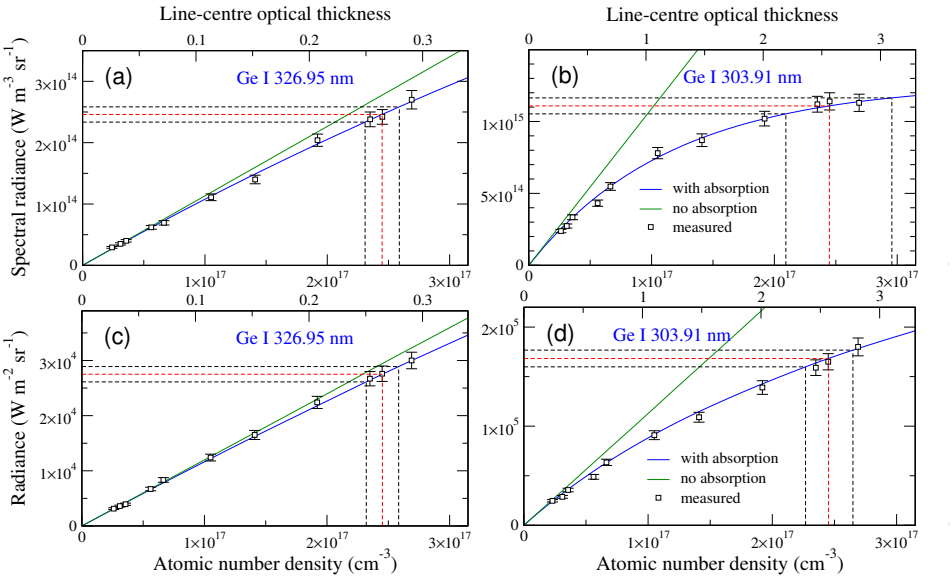

Figure 1.4: Line-center spectral radiance (a,b) and line-integrated radiance (c,d) as functions of the Ge atomic number density and τ_0 (secondary x-axis) for weakly (a,c) and stronly (b,d) self-absorbed lines. The measurement was performed in argon on a Si/Ge thin film of compositional gradient. The blue and green curves are the line intensities computed for a uniform plasma in LTE considering and ignoring self-absorption, respectively. The analytical measurement error is indicated for an intensity measurement error of 5% (Adapted from Taleb et al. [39]).

tively (see Section 1.3.4.1). In case of small optical thickness (a,c), moderate intensity lowering due to self-absorption is observed, and the relative error of the analytical measurement equals the relative error of the intensity measurement. When the optical thickness increases, the line-center intensity saturates (b), and the analytical measurement error increases exponentially. The intensity saturation is not observed for line-integrated intensity measurements (d) where a square-root dependence is expected in the regime of large optical thickness [39].

The results presented in Figure 1.4 illustrate that self-absorption must be considered in accurate CF-LIBS measurements, even for lines of small optical thickness. The measurement accuracy with self-aborbed lines depends on the line shape and on the way the intensity is measured [39]. Accurate measurements with strongly self-absorbed lines are only possible for line-integrated intensity measurements, when the line-width and the plasma size along the line of sight are precisely known.

1.2.5. Chemical reactions

Chemical reactions are mostly ignored in calibration-free LIBS analysis, although emission bands of molecules formed by chemical reactions are often observed in LIBS experiments [45]. This is justified by the typical temperature of LIBS plasmas of about 1×10^4 K, for which most of the molecular species have negligible number densities.

To illustrate the role of chemical reactions, the number densities of atomic and molecular species computed for an atmospheric Ti-sapphire plasma in LTE are displayed in Figure 1.5. It is shown that AlO molecules dominate the plasma composition at low temperature, while they have negligible abundance for $T > 6000$ K. The AlO emission emission bands observed in several studies [24, 46] are thus expected to originate from the plasma border, where the temperature is low enough to enable molecular recombination [29]. As the calibration-free LIBS measurements exploit the atomic emission originating essentially from the hot plasma core, chemical reactions can thus be ignored, as long as the molecular bands emitted from the plasma border do not interfer with the analytical lines.

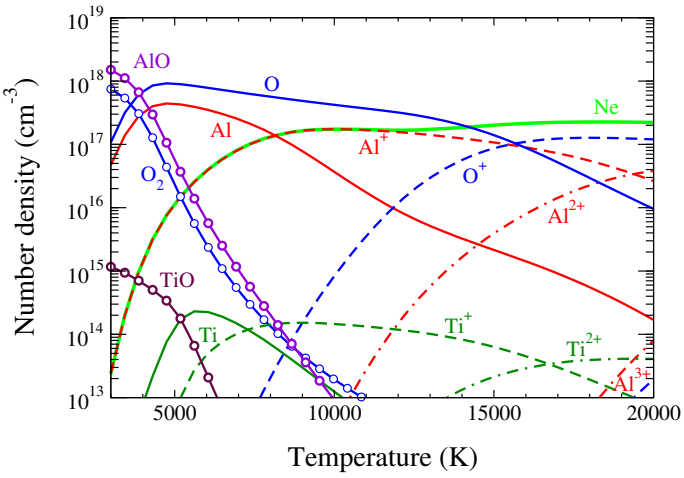

Figure 1.5: Number densities of species vs temperature computed for a plasma in LTE at atmospheric pressure, with the elemental composition of a Ti-sapphire crystal (Adapted from Hermann et al. [29]).

The situation is expected to differ from the above presented scenario of AlO formation, when chemical reactions lead to the formation of molecules with larger dissciation energy, such as CN or CO. Indeed, when the molecular dissociation energy is comparable to the ionization energy of the dominant plasma species, the presence of molecules is not limited to the cold plasma border, but extended to the hot core. Chemical reactions are thus expected to play a significant role in calibration-free LIBS analyses of organic materials, in particular when trace elements are quantified from spectral recordings with large gate delay [47]. The contribution of molecular species formed by chemical reactions in an organic equilibrium plasma is illustrated in Figure 1.6, where the number densities of atoms, ions and molecules are displayed as functions of temperature. It is shown that molecular species dominate the plasma composition for $T < 7500$ K. An overview on the role of chemical reactions in LIBS plasmas was given by De Giacomo and Hermann [45].

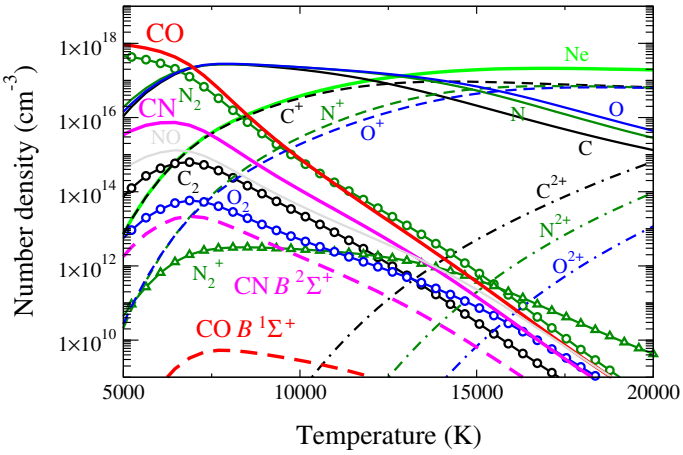

Figure 1.6: Number densities of species vs temperature computed for a plasma in LTE at atmospheric pressure composed of carbon, nitrogen and oxygen with equal atomic fractions (Adapted from De Giacomo and Hermann [45]).

1.3. Methods of calibration-free measurements

1.3.1. The mathematical problem of a multi-elemental equilibrium plasma

The state of an M elements-composing plasma in local thermodynamic equilibrium depends on $M+1$ parameters: the temperature and the atomic number densities of the M elements. In high-temperature plasmas, polyatomic molecules have negligible abundance and the atomic number density of an element A is given by

$$n_A = \sum_{z=0}^{z_{max}} n_A^z + 2\sum_{z=0}^{1} n_{A_2}^z + \sum_{B\neq A}\sum_{z=0}^{1} n_{AB}^z. \tag{1.1}$$

Here, n_A^z and $n_{A_2}^z$ are the number densities of atomic and homonuclear diatomic species of charge z, respectively, n_{AB}^z are the number densities of heteronuclear diatomic species of charge z, formed by chemical reactions with the element B. The sum includes all species of significant abundance up to the maximum charge z_{max}. The number densities of diatomic molecules formed by chemical reactions between the elements A and B are obtained from the Guldberg-Waage law of mass action [48]

$$\frac{n_A^0 n_B^0}{n_{AB}^0} = \frac{(2\pi\mu kT)^{3/2}}{h^3} \frac{Q_A^0 Q_B^0}{Q_{AB}^0} e^{-D_0/kT}, \tag{1.2}$$

where Q_A^0 and Q_B^0 are the partition functions of neutral atoms of elements A and B, respectively. Q_{AB}^0 is the partition function of the diatomic molecules formed by chemical reactions between both elements, D_0 is its dissociation energy in the ground state, $\mu = m_A m_B/(m_A + m_B)$ is the reduced mass, and k is the Boltzmann constant. Solving numerically the equations that govern the LTE plasma [49], the number densities of all plasma species are obtained quasi instantaneously from the given values of temperature and atomic number densities n_A of the M elements. Assuming charge neutrality, the electron density is obtained by summing the densities of all charged particles

$$n_e = \sum_A \sum_{z=1}^{z_{max}} z \; n_A^z. \tag{1.3}$$

For practical application, the atomic number densities n_A (Equation 1.1) of the M elements can be replaced by an equivalent set of input parameters: the electron density and the atomic or mass fractions of $M - 1$ elements. The

atomic fraction of each element C_A is

$$C_A = n_A / n_{tot}, \tag{1.4}$$

with $n_{tot} = \sum_A n_A$. Substituting the number densities in Equation (1.4) by the corresponding mass densities, we obtain the mass fractions of elements. Thus, an M elements-composing equilibrium plasma is entirely described by $M+1$ parameters: the temperature T, the electron density n_e, and the $M-1$ elemental fractions C_A. Calibration-free LIBS measurements require therefore $M+1$ measurements, involving at minimum $M+1$ spectral lines. At least one line has to be observed for each of the M elements to determine their relative fractions. At least one additional line is required to measure the temperature from the relative intensities of two transitions that belong to the same element. The electron density can be deduced from Stark broadening of one of the lines already used for fraction or temperature measurements, if the Stark broadening parameters are known and the line width is measurable.

According to the statistical laws that govern the equilibrium state, namely the Boltzmann and Saha equations, the population number densities of plasma species have exponential dependence on temperature and on the enthalpie required for their formation. It is therefore common to present their distribution in a so-called Boltzmann diagram [50, 51]. In such a diagram, the population number densities are substituted by the experimentally accessible line emission coefficients using

$$\epsilon_{ul} = \frac{hc}{4\pi\lambda} A_{ul}\, n_u, \tag{1.5}$$

where h is the Planck constant, c is the vacuum light velocity, A_{ul} is the Einstein coefficient of spontaneous emission, λ is the wavelength, and n_u is the

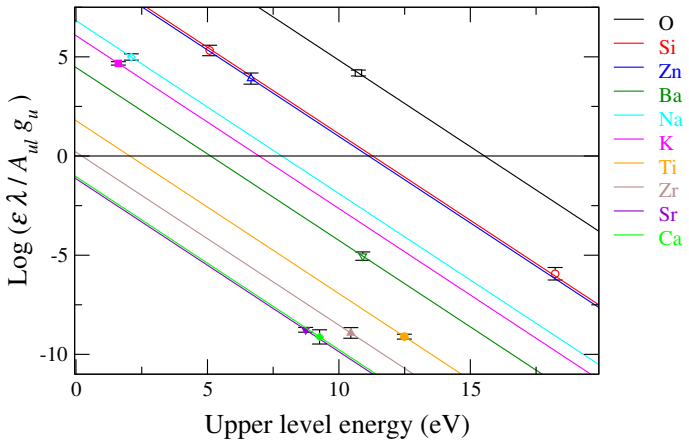

Figure 1.7: Boltzmann diagram of a plasma produced by laser ablation of barite crown glass.

upper level population number density. As an example, the Boltzmann diagram of a plasma produced by laser ablation of barite crown glass is displayed in Figure 1.7. The $M+1$ indicated transitions correspond to the calibration-free measurements reported by Gerhard et al. [28].

1.3.2. First CF-LIBS method for ideal plasma

Ciucci et al. [1] were the first to exploit the model of local thermodynamic equilibrium for direct analytical measurements. With respect to the physical model represented by the Boltzmann diagram in Figure 1.7, the authors made a simplifying assumption: the measured line intensity was supposed to be proportional to the emission coefficient. This apparently insignificant simplification has great consequences for the application of the method. On one hand, it greatly simplifies the implementation, rendering the measurements accessible through the straightforward construction of Boltzmann diagrams from the

measured line intensities. This makes the method accessible to a large community of scientists. On the other hand, the method ignored a fundamental mechanism of atmospheric equilibrium plasmas : self-absorption [52, 5]. The limitation to the ideal case of negligible self-absorption lowers considerably the analytical performance of the method.

Although well known in the community of plasma scientists, the problem of self-absorption was somehow, at least, partially hidden by the Boltzmann plot methodology. To minimize measurement errors due to inaccurate spectroscopic data (A_{ul}-values) or an unprecisely known apparatus response, Ciucci et al. recommanded to set up the Boltzmann diagram with large numbers of spectral lines for each element. Applying this statistical approach, the sources of errors were not distinguished. In addition, the ordinate of the Boltzmann plot is a logarithmic function of the emission coefficient, and large errors are naturally attentuated. In other words, even input data affected by large errors will produce in most cases a Boltzmann diagram of reasonable temperature.

Originally implemented as a tool for checking equilibrium distributions, the Boltzmann diagram is due to the loagrithmic scale not the adequate feedback for accurate concentration measurements.

1.3.3. Ammended methods

After the invention of CF-LIBS, the large dissemination of its application for analyses of various materials brought rapidly the conscience of the limited analytical performance. Due to the difficulty of identifying the dominating error sources, ammended approaches have been proposed to correct for all possible causes of failure. We can classify them in three categories : (i) corrections

not required in typical LIBS conditions; (ii) corrections required in particular cases; (iii) mandatory corrections.

According to Section 1.2.1, the correction for non-stoichiometric sample vaporization belongs to the first category. Non-stoichiometric vaporization is expected for laser irradiation with low fluence, close to the threshold of ablation, when vaporization occurs through the mechanism of thermal evaporation mainly. To get a plasma of high brilliance, LIBS is generally operated with a laser fluence of about two orders of magnitude above the ablation threshold, and the corrections proposed by Fornarini et al., Pershin and Colao were therefore rarely applied [7, 8].

The methods to account for the failure of equilibrium (see Section 1.2.2) also belong to the first category of corrections. Only a few studies report on collisional-radiative modeling of LIBS plasmas [30, 53, 54]. They concern sample materials of simple elemental composition only. Based on the calculation of the rates of all individual collisional and radiative processes, these approaches demand lots of data that are unavailable for many elements. Their use is therefore avoided by chosing the experimental conditions that favor the formation of a plasma in equilibrium.

Several approaches have been proposed to account for the nonuniform spatial distributions of temperature and densities within the laser-produced plasma. Most of them [14, 35, 36] were based on the simple scheme proposed by Hermann et al. [5] that consists to describe the plasma by two uniform zones, representing the hot plasma core and the cold border, respectively. Based on the analytical solution of the radiation transfer equation, these aproaches take benefit from fast calculation. Compared to the uniform case, the number of parameters is increased, rendering the automisation of the calibration-free LIBS

measurements challenging [36].

Some approaches have been proposed for a more accurate geometrical description of the nonuniform plasma [11, 55, 15]. However, the benefit of these approaches compared to the simple two-zone model was found to be neglibible for most transitions [56]. Significant differences in the computed line intensities and shapes were observed for strongly self-absorbed lines only. In the opposite case of weak absorption, the correction for nonuniform spatial distribution is not mandatory, as the emission originates essentially from the hot plasma core that can be considered as uniform (see Section 1.2.4).

In practice, corrections for plasma nonuniformity are rarely applied as their implementation greatly increases the complexity of calibration-free LIBS analysis. The use of argon background gas was shown to render the spatial distributions of plasma temperature and densities almost uniform [33, 34], enabling thus accurate CF-LIBS analysis with the simple uniform plasma model [57, 58]. The approaches of nonuniform plasma modeling belong thus to the above mentioned second category of corrections that are required in particular cases.

Most of the proposed amended methods of calibration-free LIBS focus on the correction for self-absorption. Absorption and emission being naturally correlated (see Section 1.2.4), the choice of the analytical transitions is governed by the compromise between largest signal-to-noise ratio and lowest optical thickness. Self-absorption changes the measured line intensity, even for small optical thickness (see Figure 1.4). The correction of self-absorption belongs thus to the third category of mandatory corrections.

As mentioned above, the correction for self-absorption is generally incorporated in the approaches of nonuniform plasma modeling, where the absorbing cold plasma border is of particular interest. However, most amended approaches ac-

counting for self-absorption consider the spatially uniform plasma. The physical model behind these approaches is therefore similar, and differences come from the simplifying assumptions concerning the spectral line shape and the computational algorithm only. The main difference lies thus in the time of calculation whereas the results are expected to be similar.

1.3.4. Methods based on spectra simulation

Hahn and Omenetto [59] quoted *"The ideal outcome would be a simulation of the spectrum"* but estimated *"that this is a nearly impossible task"*, referring to the complexity of processes associated to the generation of laser-produced plasma emission and the computational difficulties resulting from the incomplete databases. Their conclusion was certainly just when applied to the global problem of simulating emission from any element, in the entire observable spectral window from the ultraviolet to the near infrared range, and from LIBS plasmas generated under any experimental conditions.

The purpose of the present section is to show that, for measurements in appropriate experimental conditions, the simulation of LIBS spectra is not only possible, but presents the most efficient way to operate calibration-free LIBS measurements.

The term *"simulation"* is generally associated to time-expensive calculations, such as fluid dynamics calculations of plume expansion [60, 61], numerical integration of radiation transfer [15], Monte-Carlo modeling [62, 36], or kinetic or collisional-radiative modeling [30, 54]. The situation is different when the simulation of the plasma emission spectrum is based on the calculation of the spectral radiance using an anytical solution of the radiation transfer equa-

tion [5]. Assuming local thermodynamic equilibrium, this type of simulation is quasi-instantaneous and therefore of particular interest for the implemenation in iterative calcuation loops for plasma diagnostics or compositional measurements. The principle of such a method will be presented in the following section.

1.3.4.1. Calculation of spectral radiance

In appropriate experimental conditions (see Section 1.2.3), the laser-ablated vapor plume can be considered as a spatially uniform plasma. Assuming local thermodynamic equilibrium, the spectral radiance, obtained from the integration of the radiation transfer equation, is given by [52]

$$B_\lambda = B_\lambda^0(1 - e^{-\alpha(\lambda)L}), \tag{1.6}$$

where B_λ^0 is the blackbody spectral radiance, $\alpha(\lambda)$ is the absorption coefficient, and L is the plasma size along the line of sight. The optical thickness is given by $\tau = \int \alpha(z)dz = \alpha L$. In the optically thin case ($\tau \ll 1$), Equation (1.6) becomes

$$B_\lambda = \varepsilon_\lambda L, \tag{1.7}$$

where the emission coefficient ε_λ is related to the absorption coefficient via Kirchhoff's law of thermal radiation $\varepsilon_\lambda/\alpha = B_\lambda^0$. In the opposite case of large optical thickness ($\tau \gg 1$), Equation (1.6) simplifies to

$$B_\lambda = B_\lambda^0. \tag{1.8}$$

The spectral radiance becomes independent of the plasma size, and depends on temperature only. Considering all relevant transitions between bound and free excitation levels, the absorption coefficient writes

$$\alpha(\lambda) = \sum_i \alpha_{line}^{(i)}(\lambda) + \alpha_{ion}(\lambda) + \alpha_{IB}(\lambda), \tag{1.9}$$

where the sum includes the absorption coefficients $\alpha_{line}^{(i)}$ of transitions between bound levels. The terms $\alpha_{ion}(\lambda)$ and $\alpha_{IB}(\lambda)$ account for absorption through radiative ionization and inverse bremsstrahlung, respectively. The absorption coefficient of transitions between bound levels is given by [63]

$$\alpha_{line}(\lambda) = \pi r_0 \lambda^2 f_{lu} n_l P(\lambda) \left(1 - e^{-hc/\lambda kT}\right), \tag{1.10}$$

where r_0 is the classical electron radius, and f_{lu} is the absorption oscillator strength of the transition. The lower level population number density n_l depends via the Boltzmann law on the total number density of the emitting species, and via the set of Saha equations on the total atomic number density (see Equation 1.1) and thus on the elemental fraction (see Section 1.3.1).

The normalized line profile $P(\lambda)$ is calculated considering Doppler and Stark effects, that are the dominant mechanisms of line broadening in strongly ionized laser-produced plasmas [64]. Depending on their relative contributions, the line shape is described by Gaussian, Lorentzian or Voigt profiles. For rapid calculation, the Voigt profile, that is the convolution between Gaussian and Lorentzian functions, is substituted by the so-called *Pseudo-Voigt* profile [65]. To compare measured and computed spectra, the spectral radiance computed according to Equation (1.6) is convoluted with the apparatus spectral profile $P_{ap}(\lambda)$ and corrected by an apparatus-dependent numerical factor $R_{ap}(\lambda)$,

called apparatus response. The measured intensity is

$$I(\lambda) = R_{ap}(\lambda) \int_0^\infty P_{ap}(\lambda - \lambda') B_\lambda \, d\lambda'. \tag{1.11}$$

For illustration, spectra recorded for laser ablation of steel are displayed in Figure 1.8 (a) for two different times. They are compared to computed spectra for three narrow spectral windows in which the most intense emission lines are shown to saturate at the blackbody spectral radiance (b), as expected for strongly self-absorbed transitions emitted from a uniform LTE plasma (see

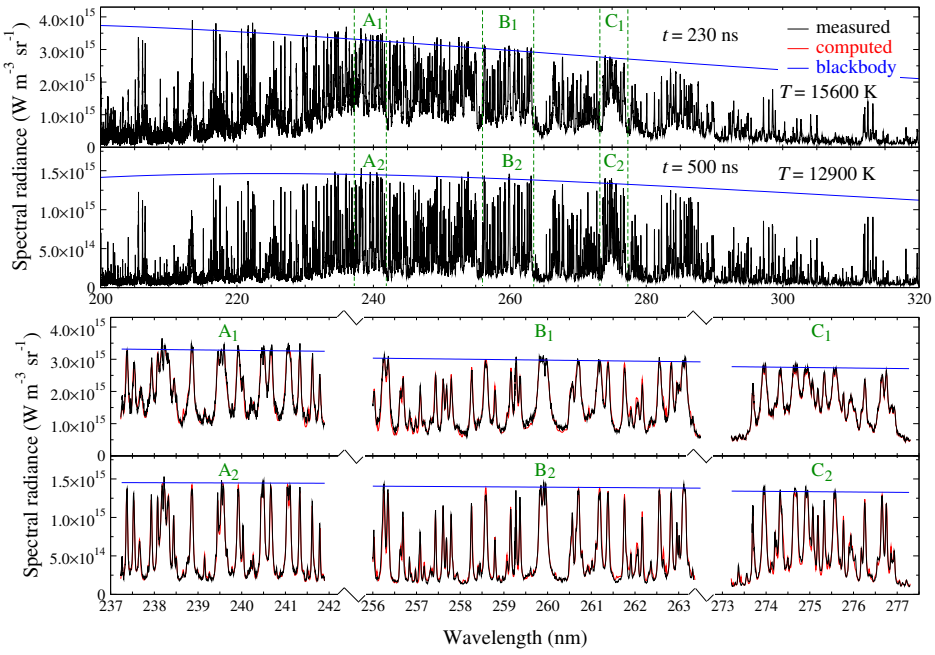

Figure 1.8: Spectra recorded during laser ablation of steel in argon at different times. The strongest transitions are shown to saturate at the blackbody spectral radiance. The temperature was deduced from the intensity distribution of optically thin lines. The excellent agreement with the spectral radiance computed using Equation (1.6) shows that the emission originates from a uniform plasma in LTE. (Adapted from Hermann et al. [34])

Equation 1.8).

1.3.4.2. Implementation in measurement algorithm

The calculation of the spectral radiance is implemented in an iterative algorithm to operate the calibration-free LIBS measurements. The algorithm is based on two loops of iteration, as shown by the scheme presented in Figure 1.9. In the principal loop (a), the parameters that characterize the plasma, namely the electron density, the temperature, the elemental fractions, and the plasma size along the line of sight, are measured successively. Each measurement is operated using the calculation loop (b) by comparing the computed spectrum to the measured one while varying the parameter of interest. The corresponding parameter is deduced from the best agreement between measured

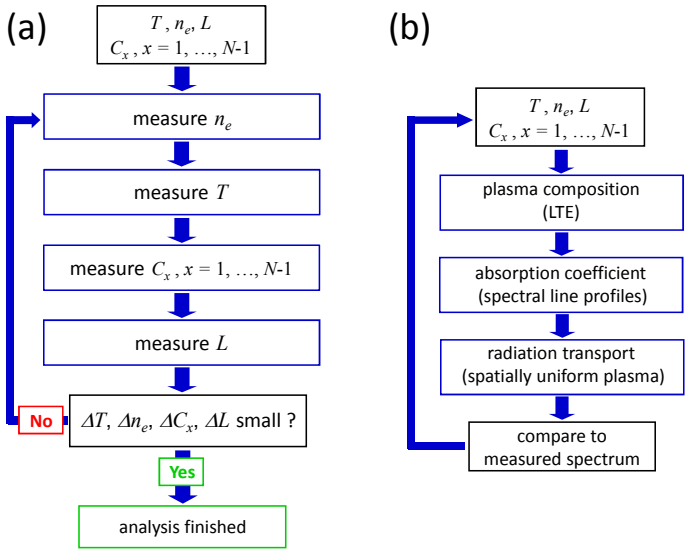

Figure 1.9: Algorithm of calibration-free LIBS analysis: (a) principal iteration loop with successive measurements of electron density, temperature, elemental fractions, and plasma diameter. Each measurement is performed using the calculation loop (b) by varying the parameter to be measured. (Adapted from Chen et al. [47])

and comuted spectra by minimizing

$$\chi^2 = \sum_i \frac{[I_{meas}(\lambda_i) - I_{comp}(\lambda_i)]^2}{I_{comp}(\lambda_i)}, \tag{1.12}$$

as shown in Figure 1.10 for the measurement of the plasma size in calibration-free LIBS analysis of barite crown glass [28].

The calculation is started with arbitrary values of parameters, for example $n_e = 1 \times 10^{17}$ cm^{-3}, $T = 1 \times 10^4$ K, $L = 1.0$ mm, and equal elemental fractions. The principal loop (a) is started with the electron density measurement via Stark broadening of an appropriate spectral line. The choice of measuring n_e prior T is motivated by the weak dependence of the Stark width on temperature. Next, the temperature is measured via the intensity ratio of spectral

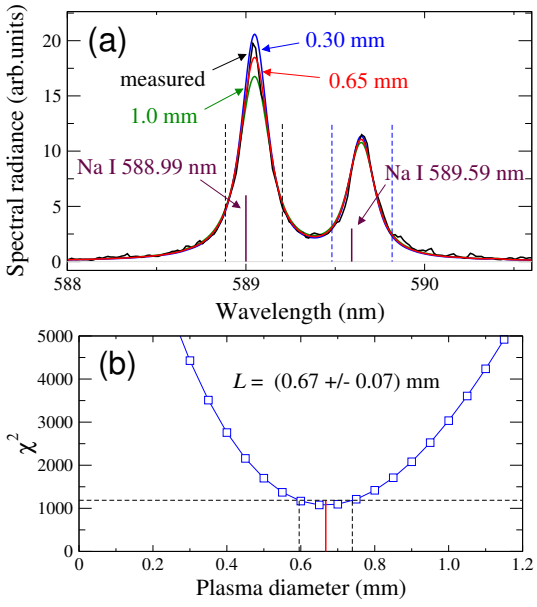

Figure 1.10: (a) Measured spectrum and spectral radiance computed for different values of plasma size. (b) The effective L-value is deduced from the best agreement via the χ^2-test according Equation 1.12. (Adapted from Gerhard et al. [28])

lines emitted from species that belong to the same element, having a sufficiently large gap between their upper level energies. Third, the fractions of major, minor and trace elements are measured consecutively. Last, the plasma size is deduced from the intensity ratio of two transitions of the same species with significantly different optical thicknesses, and preferentially similar values of upper and lower level energies (see Figure 1.10). The measurement loop is executed until the changes of temperature, electron density, elemental fractions, and plasma diameter are small compared to their absolute values.

1.3.4.3. Illustration for alloy

The calibration-free analysis is illustrated for 20 euro cent coins made from a brass alloy called *nordic gold*. It is composed of copper, aluminum, zinc, and tin with mass fractions of 89%, 5%, 5% and 1%, respectively. In addition to the alloy-composing elements, the coins contain several trace elements. Analyzing coins of different origins and manufacturing dates, the fractions of major and most trace elements were found to be equal for all coins [66]. Differences appear for nickel and manganese : compared to coins manufactured in 1999, the nickel content is about 5 times lower for the coins manufactured in 2000 and later. The change of composition is independent of the manufacturing country as shown in Figure 1.11. It is attibuted to the evolution of the European regulation towards more rigorous limitation of the use of hazardous elements.

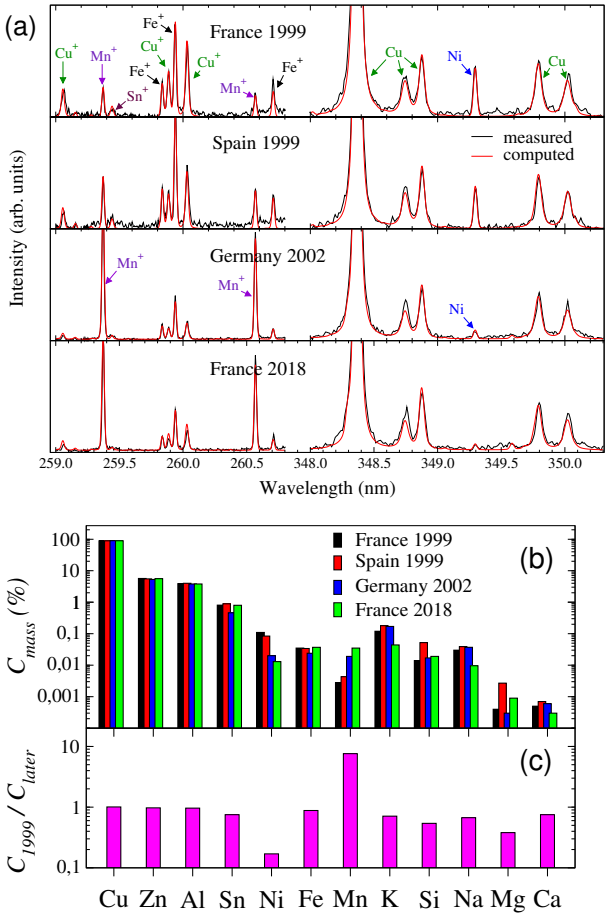

Figure 1.11: (a) Spectra recorded for 20 euro cent coins of different origins and manufacturing dates. (b) Mass fractions of elements deduced from LIBS measurements. (c) Ratio between fractions of coins manufactured in 1999 and of those fabricated afterwards.

1.4. Critical review of analytical performance

1.4.1. Model validity

It is not an easy task to conclude on the analytical performance of calibration-free LIBS from the numerous results reported in literature over more than two decades. The reason is that they have been performed in a large variety of experimental conditions, using different calibration-free LIBS measurement methods. Globally, *pure* calibration-free LIBS seems to suffer an analytical performance that does not satisfy the users. This is illustrated by the recent trend to combine CF-LIBS with the calibration using a single standard sample [16, 17, 18]. According to the authors, the single calibration step aims to compensate errors due to spectroscopic data and the unprecise knowledge of the apparatus response.

Calibration-free LIBS is often considered as accurate for major elements, and less accurate for minor and trace elements. It is obvious that this trend cannot be attributed to a lack of validity of the physical model. Nonstoichiometric ablation or failure of equilibrium depends on the physical properties of the element, but not on its abundance. We can therefore conclude from the numerous successful measurements of major elements, that the analytical performance of calibration-free LIBS is not limited by the failure of the model.

This does however not mean that many reported results suffer low accuracy due to a lack of model validity, caused by the choice of inappropriate experimental conditions. For example, in many experiments, recordings are performed with a large detector gate width to obtain spectra of highest signal-to-noise

ratio [67, 68, 16, 69, 70, 71, 72]. In that condition, failure of model validity is expected due to two distinguished causes: (i) according to the rapid time-evolution of the plasma, the temperature will significantly change during the time of observation. As the spectral line intensity dependence on T is non-linear, the use of an average temperature leads to measurement errors. (ii) A large detection gate width includes late times for which the electron density may be too low to ensure LTE validity.

1.4.2. Error evaluation

1.4.2.1. Minor and trace element quantification

It is often postulated that the large errors of minor and trace element measurements in calibration-free LIBS analysis are due to the so-called *closure relation*, imposing that the sum of all elemental fractions equals 100%. As a consequence of the closure condition, small errors associated to elements of large abundance are supposed to generate large errors for minor and trace elements [43].

This error prediction should be supported mathematically by the dependence of the elemental fraction on the intensity of the analytical signal. According to Equation 1.4, the elemental fraction C_A does not only depend on the atomic number density of the element n_A but also on the atomic number densities of all other sample-composing elements. Applying the standard procedure of error propagation based on the partial derivates with respect to the atomic number densities n_j, the relative error of the elemental fraction is given by [39]

$$\frac{\Delta C_A}{C_A} = \sqrt{(1-C_A)^2 \left(\frac{\Delta n_A}{n_A}\right)^2 + \sum_{j \neq A}^{N} C_j^2 \left(\frac{\Delta n_j}{n_j}\right)^2}. \tag{1.13}$$

Neglecting self-absorption, the intensity I_j is proportional to n_j (see Section 1.3.1). Ignoring furthermore all error sources, except the error associated to the measurement of analytical signal intensity, the relative errors of the atomic number densities $\Delta n_j/n_j$ can be substituted by the corresponding intensity measurement errors $\Delta I_j/I_j$.

The first term in the quadratic sum represents the contribution of the analytical signal measurement error associated to the proper element A. The weighting by the factor $(1 - C_A)^2$ shows that this contribution decreases with increasing C_A. Contrarily, the contributions of errors associated to the analytical signal measurement of the other elements increase with the corresponding fractions C_j.

In the case of a single element material containing only very small fractions of other elements ($C_A \to 1$), the fraction measurement error of the major element tends towards zero. In the opposite case of very small elemental fraction, we have $1 - C_A \cong 1$. The error contribution of the analytical signal of element A is weighted by unity. The error contributions due to the analytical signal measurements of the other elements are weighted by their mass fractions. Assuming similar signal measurement errors for all elements, the contributions of the signal measurement errors of the other elements are always smaller than the contribution of the signal measurement error of element A.

Thus, the errors of minor or trace elements are moderately impacted by the measurement errors of major elements, and the *closure relation* does not explain apparently large measurement errors of elements having small abundance. An alternative explanation for the low measurement accuracy of minor and trace element fractions can be given by the error associated to the signal-to-noise ratio. To satisfy the LTE validity condition, calibration-free LIBS mea-

surements must be performed in conditions of sufficiently large electron density. The large charge density is associated to intense continuum emission due to bremsstrahlung and radiative recombination. Low intensity spectral lines are thus hidden by the continuum, and the quantification of minor and trace elements is challenging. The problem is even enhanced when organic materials are investigated. Composed in majority of carbon, hydrogen, nitrogen and oxygen, the LTE validity condition is particularily severe. These atoms have large energy gaps in their atomic structures, and the establishment of Boltzmann equilibrium distributions of their population number densities require a large electron density according to the criterion of McWhirter [22].

To improve the accurary of minor and trace element evaluation in calibration-free LIBS analysis, Chen et al. [47] proposed a measurement procedure based on the exploitation of two spectra, recorded with different gate delays (see Figure 1.12). The early spectrum is recorded for a time, when the electron density is large enough to ensure full LTE conditions. This spectrum is used to determine the fraction of major and minor elements. The late spectrum is recorded for conditions of partial equilibrium, when the electron density is significantly reduced, and Boltzmann equilibrium distributions are established for metal atoms only. This spectrum serves to measure the relative amount of minor and metal trace elements. The method was applied to measure trace elements in seafood [47], and more recently to quantify impurities in optical glass [58] (see Chapter 22 for details).

An additional error of trace element measurements can be attributed to the probe volume. Indeed, the fractions of trace elements at the surface and in the bulk often differ and the probe volume of CF-LIBS analysis may not represent the bulk material composition [58]. Advanced CF-LIBS measurement proce-

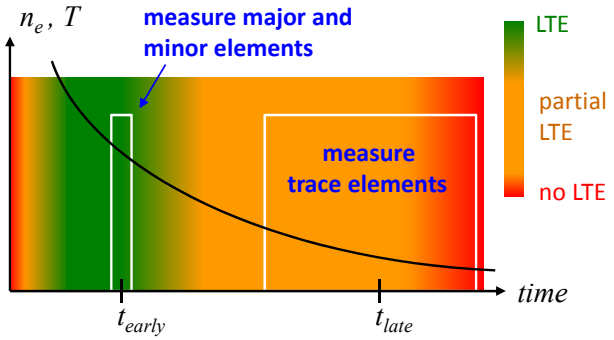

Figure 1.12: Time scheme of procedure for sensitivity-improved CF-LIBS analysis: two spectra are recorded at different times. The early recording in conditions of full LTE serves to quantify major and minor elements. The late recording in conditions of partial LTE serves to measure minor and trace elements. The color scale from green to red indicates the degree of equilibrium. (Adapted from Chen et al. [47])

dures include therefore a surface cleaning step, that consists in the irradiation of the sample with one or several laser pulses prior spectra recording.

1.4.2.2. Error due to self-absorption

Self-absorption is generally considered as a drawback and a source of measurement errors. In plasma diagnostics, the *golden rule* is to use transitions of moderate optical thickness only ($\tau \leq 1$), for which corrections of intensity or width measurements are possible with reasonable associated errors [73]. Recently, several authors presented a different view of self-absorption, proposing solutions that enable corrections in case of large optical thickness [43, 44], or presenting self-absorption as an advantage for plasma diagnostics [41, 42, 74]. The physical problem is illustrated in Figure 1.4 by the decrease of the slope of the curves-of-growth with the optical thickness. The analytical measurement error depends on the slope of the curve-of-growth and on the uncertainty of its computational reproduction via Equation 1.6. Applying the rigorous formalism

of error propagation, we can derive from Equation 1.6 the following expression of the analytical measurement error [39]

$$\frac{\Delta n_A}{n_A} = \sqrt{\left(\frac{\Delta \tau_0}{\tau_0}\right)^2 + \left(\frac{\Delta A_{ul}}{A_{ul}}\right)^2 + (1 - e^{-\tau_0})\left(\left(\frac{\Delta w_{sd}}{w_{sd}}\right)^2 + \left(\frac{\Delta L}{L}\right)^2\right)}. \tag{1.14}$$

Here, w_{sd} is the spectral line width, Δw_{sd} is its uncertainty, ΔA_{ul} and ΔL are the errors associated to the transition probability and the plasma size, respectively. The factor $1-e^{-\tau_0}$ is inserted empirically to retrieve the expression for the optically thin case ($\tau_0 \ll 1$) for which the analytical measurement accuracy is not impacted by the line width and the plasma size. The error $\Delta\tau_0$ is obtained from the $I = f(\tau_0)$ dependence obtained from Equation 1.6 via the derivative of the inverse function. We have

$$\frac{\Delta \tau_0}{\tau_0} = \frac{1}{\tau_0}\frac{f(\tau_0)}{f'(\tau_0)}\frac{\Delta I}{I} \equiv g(\tau_0)\frac{\Delta I}{I}, \tag{1.15}$$

where $f'(\tau_0) \equiv \partial I/\partial \tau_0$. The error growth factor $g(\tau_0)$ is introduced to account for the increase of measurement uncertainty due to self-absorption. For line-center intensity measurements, the error growth factor is obtained in case of neglibile apparatus broadening directly from Equation 1.6 as

$$g_0 = \frac{1 - e^{-\tau_0}}{\tau_0\, e^{-\tau_0}}. \tag{1.16}$$

For measurements of the line-integrated intensity, no analytical expression $I_{line} = f(\tau_0)$ exists for common line shapes represented by the Voigt profile, and the error growth factor is obtained from Equation 1.15 using the numerically calculated derivative $f'(\tau_0)$.

The error growth factor is presented in Figure 1.13 as a function of τ_0 for line-

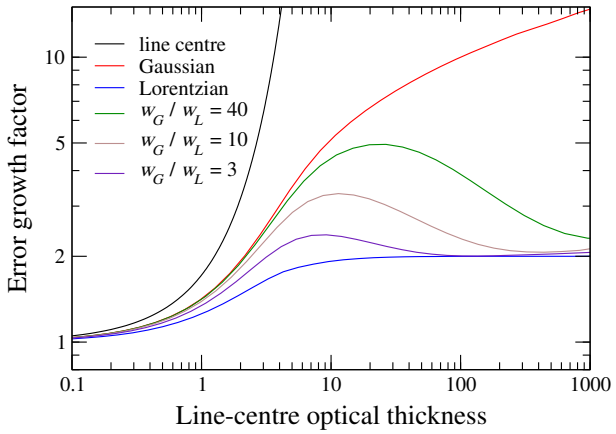

Figure 1.13: Error growth factor vs τ_0 computed according Equation 1.15 for I_0-measurements (black curve) and I_{line}-measurements of line profiles with different ratios of Gauss width w_G over Lorentz width w_L (colored curves) (Adapted from Taleb et al. [39]).

center and line-integrated intensity measurements. A moderate error growth by $g \leq 2$ is observed for I_{line}-measurements with Lorentzian line shapes. The error increases with the Gaussian contribution to the line profile. However, the error amplification due to the Gaussian contribution diminishes for very large τ_0-values until it vanishes, and we retrieve the value $g \simeq 2$ of the Lorentzian line shape. This behavior is attributed to the small wings of the Gaussian profile that limit the contribution to a narrow spectral range close to the resonance wavelength, in which saturation at the blackbody spectral radiance occurs. The Lorentzian contribution dominates thus at very large τ_0-values, according to the large Lorentzian line wings.

In typical conditions of LIBS experiments, spectral lines have a Doppler width of a few pm, and a Stark width ranging from picometers to nanometers. Thus, in most cases, the error growth factor is situated between the g-values of the pure Lorentzian profile and those observed for profiles with Gaussian contri-

bution $w_G/w_L = 3$ (see Figure 1.13). The error of the line-integrated intensity if thus increased moderatly by $g \simeq 2$ for $\tau_0 \gg 1$.

As the amount of absorption depends on the spectral line width and the plasma size along the line of sight, the analytical measurement error is increased by the contributions of Δw_{sd} and ΔL, when self-absorbed lines are used (see Equation 1.14). In most cases, line width and plasma diameter are known with moderate or low accuracy, and analytical measurements with strongly self-absorbed lines are generally affected by large measurement errors.

1.4.3. Recommendations

1.4.3.1. Apparatus requirements

Spectrometer. Compared to LIBS analysis based on calibration with standard samples, calibration-free LIBS measurements have additional requirements for the used equipment. First of all, all elements of significant abundance have to be quantified, and the CF-LIBS apparatus has thus to cover a large spectral window, to ensure that spectral lines of all elements are observable. Second, the resolving power of the spectrometer has to be large enough to minimize line interferences, and to enable electron density measurements via Stark broadening of spectral lines. Both requirements are satisfied by using echelle spectrometers that were designed to combine the broadband spectral window with the high resolving power.

Motorized sample holder. Echelle spectrometers suffer low sensitivity, and the recording of spectra with sufficiently large signal-to-noise ratio requires therefore signal acquisition with large repitition numbers. Based on plasma modeling for given values of temperature and electron density, calibration-

free LIBS measurements have to be operated in reproducible conditions of laser-material interaction. Thus, the number of laser pulses applied to the same irradiation site on the surface of the sample has to be small enough, to prevent the change of the plume expansion dynamics due to the so-called *canon effect*. To preclude the canon effect, the depth of the laser-produced crater has to be small compared to its diameter. Depending on the material properties, a number of 5, 10 or 20 laser pulses can be typically applied to the same irradiation site. As spectra of sufficiently large signal-to-noise ratio require signal accumulation over a number of about 100 ablation events, it is recommended to use a motorized sample holder that enables automized positioning for recordings on multiple irradiation sites.

Apparatus response correction. For the comparison with the plasma emission predicted by the LTE model, the measured spectrum has to be corrected by the apparatus response function. The apparatus response function is measured with radiation standards, such as deuterium arc and tungsten filament lamps for the ultraviolet and visible/near infrared spectral ranges, respectively. For echelle spectrometers, these measurements are challenging due to the strong intensity variation of the calibration standard radiation over the boadband spectral window [75]. In particular, difficulties arise when using low power tungsten lamps, due to the weak emission intensity in the spectral range $<$ 500 nm.

1.4.3.2. Setting the experimental conditions

Laser irradiation.

Pulse energy. To satisfy the LTE validity condition, the plasma lifetime has to be large compared to the time required for the establishment of equilibrium. As

the plasma lifetime depends on the laser pulse energy, the request of sufficiently long plasma lifetime leads to a minimum of required laser pulse energy. To minimize the effect of self-absorption, the plasma should have a small size (see Equation 1.6). This condition imposes laser irradiation with small pulse energy. Both conditions, the need of LTE validity and the limitation of self-absorption, are typically satisfied for irradiation with ultraviolet laser pulses of a few mJ. Due to the lower energy coupling towards the material, slightly higher pulse energy may be applied when using infrared laser radiation.

Beam focusing. Focusing to a spot diameter of about 100 μm leads to a fluence of about 10^2 J cm^{-2} that is sufficiently large to ensure stoichiometric mass transfer from the solid sample towards the plasma (see Section 1.2.1).

Pulse duration. The rate of plasma heating depends on the laser intensity that increases naturally with decreasing pulse duration. However, to obtain highest rates of atomization and excitation during the typical time of LIBS spectra observation, laser heating should occur during the expansion of the vaporized sample material. The laser pulse duration should therefore be large enough. A laser pulse duration of the order of a nanosecond was found to be good compromise for optimized plasma heating [76].

Radiation wavelength. Compared to material ablation with infrared laser radiation, the effect of plasma screening is reduced when ultraviolet radiation is applied. The laser energy is therefore mostly deposited in the vapor plume, close to the sample surface. This condition is supposed to favor the formation of a spatially uniform plasma [34]. However, the most appropriate radiation wavelength for calibration-free LIBS measurements is still an open question, as it also depends on the other laser irradiation parameters and the sample

material properties.

Spectra recording.

Gate delay and gate width. The spectra must be recorded with a gated detector, using a sufficiently short delay between the laser pulse and the detector gate, so that the electron density is large enough to satisfy the LTE validity condition. In addition, the gate width Δt_{gate} must be short enough, so that the variations of plasma properties during the time of observation are negligible ($\Delta T/T, \Delta n_e/n_e \ll 1$). The choice of the gate width is thus given by a compromise between small enough variations of T and n_e, and large enough signal-to-noise ratio. This compromise was found for $\Delta t_{gate} = t_d/2$, where t_d is the delay between the laser pulse and the detector gate [57].
In particular cases, the full LTE state is not required and conditions of partial LTE may be exploited for metal trace element quantification (see Section 1.4.2.1). Accordingly, these measurements are performed in conditions of enhanced signal-to-noise ratio, using larger values of t_d and Δt_{gate}.

Signal treatment. Prior the correction by the apparatus response function, the electronic noise must be substracted from the measurement spectrum. Thus, in addition to the recording of the signal, the noise must be recorded with the same exposure time. Advanced spectroscopic instruments enable noise recording and substraction via an automized procedure.

Atmospheric conditions.

Pressure. The pressure of the background gas determines the volume and the density of the laser-ablated vapor plume. At low pressure, the density and therefore the rates of collisions are reduced. The equilibrium state is hardly

established, due to the reduced electron density and the shorter plasma lifetime. In addition, diffusion may lead to mass-dependent segregation of elements [77]. With increasing pressure, the processes of collisional quenching and self-aborption lower the radiation efficiency. A good compromise between model validity and radiation efficiency is achieved for measurements at atmospheric pressure.

Gas nature. Compared to the plume generated in ambient air, the plasma produced in argon was shown to be more appropriate for calibration-free LIBS measurements. Beside the larger values of T, n_e and the longer lifetime, the plasma in argon appears more uniform and enables therefore more accurate and straightforward modeling of the plasma emission spectrum [33, 34].

Laboratory environment. Echelle spectrometers are extremely sensitive to temperature variations and small changes of the order of 1 K may alter the spectral calibration and the apparatus response function [75]. The changes of the apparatus response may strongly impact the accuracy of the calibration-free LIBS analyses. It is therefore recommanded to work in a temperature-stabelized laboratory environment, or with a temperature-stabelized echelle spectrometer.

1.4.3.3. Selection of spectral lines

The rules for the selection of spectral lines in calibration-free LIBS include the line selection rules in calibrated LIBS and the following additional rules.

Accuracy of transition probability. Based on spectra calculation, calibration-free LIBS requires accurate spectroscopic data. The choice of the analytical lines is therefore conditioned by the accuracy of the transition probability re-

ported by the mostly used spectroscopic database of the National Institute of Standards and Technology (NIST) [78] or by other sources.

Upper level energy. Modeling based on the assumption of a uniform plasma does not account for possible spatial variations of temperature and densities. This simplification is thus equivalent to an uncertainty of temperature, that is expected to play a particular role when calibration-free LIBS measurements are performed in ambient air (see Section 1.2.3). To minimize errors due to temperature variation, the spectral lines should be chosen with upper level energies close to each others.

Wavelength. To minimize errors due to the uncertainty of the apparatus response function, the spectral lines should be preferentially chosen in a narrow spectral window. For measurements with an echelle spectrometer, the wavelength positions at the frontier between two diffraction orders should be avoided, as these positions correspond to local minima of the apparatus response for which the largest changes are expected in case of temperature variation.

Optical thickness vs signal-to-noise ratio. The choice of the analytical line for most accurate compositional measurements is guided by the compromise between the error due to self-absorption (see Section 1.4.2.2) and the uncertainty associated to the signal-to-noise ratio. The selection of the most appropriate lines can be automized via the minimization of the analytical error obtained by Equation 1.14. The advantage of calibration-free LIBS approaches via spectra simulation (see section 1.3.4) is here that the optical thickness of the spectral lines is known.

1.4.4. Expected improvements

1.4.4.1. Evolution of spectroscopic database

One of the principal sources of measurement uncertainty in calibration-free LIBS is due to missing or unprecise spectroscopic data. Indeed, Einstein coefficients of spontaneous emission are still unknown for many transitions, or known with low accuracy. The uncertainty of the A_{ul}-values impacts directly the measurement of the elemental fraction (see Equation 1.5). The composition measurement errors can be even amplified by the temperature measurement error resulting from the unprecise A_{ul}-values. Moreover, accurate Stark broadening parameters are missing for most transitions. Erros in the calculation of the line width do not only affect the comparison of computed and measured spectra, but also lead to an error in the calculation of the optical thickness, and therefore to an error in the calculation of intensity-lowering due to self-absorption.

However, the knowledge of both A_{ul}-values and Stark broadening parameters improves continuously, as illustrated by numerous recent reports on the subject and the regular updates of the NIST spectroscopic database [78]. Due to its exceptional properties, the plasma produced by laser ablation in appropriate experimental conditions represents a radiation source of great interest for such measurements [79, 80]. It is thus expected, that the errors due to unprecise spectroscopic data will progressively diminish.

1.4.4.2. Advanced instrumentation

The uncertainty of the apparatus response function is another significant error source in calibration-free LIBS analysis. Improvements are possible via the

temperature-stabelization of spectrometers, and also via new methods for the measurement of the apparatus response using the laser-produced plasma as a radiation standard.

Taleb et al. [75] presented recently a method based on the simulation of the emission spectrum of the plasma produced by laser ablation of steel, that was applied to check and and to correct the apparatus response of echelle spectrometers. Based on the comparison of measured and computed spectral line intensities, this method required a preliminary calibration with continuous radiation sources such as deuterium and tungsten lamps. The continuum emission generated by the laser-induced plasma during the early stage of expansion may present an alternative to the use of these lamps. In particular, the plasma produced by laser ablation of heavy metals, such as tungsten, is promising, due to the associated intense contimuum emission. Thus, rapid and accurate apparatus response measurements via the simple change of the sample material may present a significant advance in the methodology of future calibration-free LIBS analyses.

1.4.4.3. Improved knowledge of laser-induced plasma

Although laser-induced plasmas are under investigation since several decades, the involved phyico-chemical processes are still not fully understood. In particular, there does not yet exist a model capable to predict accurately the expansion dynamics of the laser-generated ablation plume into the ambient gas. Modeling is rather limited to the qualtitative description of the processes of laser ablation and plasma generation. It is therefore difficult to predict phenomena that impact the calibration-free LIBS analysis, such as the role of chemical reactions, spatial distributions of temperature and species densities.

Thus, experimental investigations are still required to improve our knowledge of the physico-chemical properties of the plasma for the large variety of experimental conditions typically used in calibration-free LIBS measurements. The advantages of CF-LIBS in argon background gas have been recently demonstrated [34]. However, many applications require measurements in ambient air. In that condition, plasma modeling under the assumption of a spatially uniform plasma is questionable (see Section 1.2.3) and conditioned by the optical thickness of the analytical lines. So the influence of self-absorption on the analytical performance is here of interest.

The role of chemical reactions is also mostly ignored. They may impact the calibration-free measurement result, in particular in analyses of organic materials (see Section 1.2.5). The description of the equilibrium chemistry is challenging. It opens new perspectives for the exploitation of molecular emission spectra in elemental and isotopic analyses [29, 81].

1.5. Conclusion

Direct compositional analysis through modeling of the emission spectrum of the laser-induced plasma is a unique tool in analytical chemistry. Although the analytical performances reported in literature for major, minor and trace element measurements do not yet enable a clear qualification of these methods, the here presented resultats and recent advances illustrate that calibration-free LIBS is not only a promising technique, but already presents a powerful analytical tool, when operated in appropriate experimental conditions.

Further progress is expected in the next years, in particular due to advances in instrumentation and improvements of spectroscopic data. The numerous pro-

posed algorithms and mathematical solutions for corrections of self-absorption and other features brought progress in the CF-LIBS methodolies. Compared to methods using corrections for self-absorption based on simplifying assumptions on the spectral line shapes, spectral radiance calculations based on analytical solutions of the radiation transfer equation have the advantage to account intrinsically for self-absorption. These calculations are rapid and their implementation in appropriate measurement loop enable calibration-free LIBS analyses in a time comparable to the spectra recording time of the order of a minute.
The successful dissemination of calibration-free LIBS also requires tools that facilitate its operation, as for example an easy to handle and accurate method for measuring the apparatus response function, and powerful software for the automized operation of CF-LIBS measurements.
Finally, as a result of the unique properties of the laser-induced plasma, that, in appropriate conditions, combines the features of local thermodynamic equilibrium, spatial uniformity and small size, calibration-free laser-induced breakdown spectroscopy is foreseen to have a bright future.

Bibliography

[1] A. Ciucci, M. Corsi, V. Palleschi, S. Rastelli, A. Salvetti, and E. Tognoni. New procedure for quantitative elemental analysis by laser-induced plasma spectroscopy. *Appl. Spectrosc.*, 53:960–964, 1999.

[2] S. Eliezer, A. D. Krumbein, and D. Salzmann. A generalised validity condition for local thermodynamic equilibrium in a laser-produced plasma. *J. Phys. D: Appl. Phys.*, 11(12):1693–1701, 1978.

[3] J. Hermann, C. Boulmer-Leborgne, B. Dubreuil, and I. N. Mihailescu. Influence of irradiation conditions on plasma evolution in laser-surface interaction. *J. Appl. Phys.*, 74:3071–3079, 1993.

[4] J. Hermann, A. L. Thomann, C. Boulmer-Leborgne, B. Dubreuil, M. L. De Giorgi, A. Perrone, A Luches, and I. N. Mihailescu. Plasma diagnostics in pulsed laser TiN layer deposition. *J. Appl. Phys.*, 77:2928–2936, 1995.

[5] J. Hermann, C. Boulmer-Leborgne, and D. Hong. Diagnostics of the early phase of an ultraviolet laser induced plasma by spectral line analysis considering self-absorption. *J. Appl. Phys.*, 83(2):691–696, 1998.

[6] E. Tognoni, G. Cristoforetti, S. Legnaioli, and V. Palleschi. Calibration-free laser-induced breakdown spectroscopy: State of the art. *Spectrochim. Acta Part B: Atom. Spectrosc.*, 65:1–14, 2010.

[7] L. Fornarini, F. Colao, R. Fantoni, V. Lazic, and V. Spizzicchino. Calibration analysis of bronze samples by nanosecond laser induced breakdown spectroscopy: A theoretical and experimental approach. *Spectrochim. Acta Part B: Atom. Spectrosc.*, 60:1186–1201, 2005.

[8] S. M. Pershin and F. Colao. Laser plasma emission spectrum corrected for the quantitative analysis of alloys. *Tech. Phys. Lett.*, 31:741–745, 2005.

[9] V. Lazic, R. Barbini, F. Colao, R. Fantoni, and A. Palucci. Self-absorption model in quantitative laser induced breakdown spectroscopy measurements on soils and sediments. *Spectrochim. Acta Part B: Atom. Spectrosc.*, 56:807–820, 2001.

[10] D. Bulajic, M. Corsi, G. Cristoforetti, S. Legnaioli, V. Palleschi, A. Salvetti, and E. Tognoni. A procedure for correcting self-absorption in

calibration-free laser-induced breakdown spectroscopy. *Spectrochim. Acta Part B: Atom. Spectrosc.*, 57:339–353, 2002.

[11] I. B. Gornushkin, C. L. Stevenson, B. W. Smith, N. Omenetto, and J. D. Winefordner. Modeling an inhomogeneous optically thick laser induced plasma: a simplified theoretical approach. *Spectrochim. Acta Part B: Atom. Spectrosc.*, 56:1769–1785, 2001.

[12] J. A. Aguilera, J. Bengoechea, and C. Aragón. Curves of growth of spectral lines emitted by a laser-induced plasma: influence of the temporal evolution and spatial inhomogeneity of the plasma. *Spectrochim. Acta Part B: Atom. Spectrosc.*, 58:221–237, 2003.

[13] J. Hermann. System and method for quantitative analysis of the elemental composition of a material by laser-induced breakdown spectroscopy (LIBS), Patent PCT/FR2009/001221, WO 2010/052380 A1.

[14] C. A. D'Angelo, D. M. D. Pace, G. Bertuccelli, and D. Bertuccelli. Laser induced breakdown spectroscopy on metallic alloys: Solving inhomogeneous optically thick plasmas. *Spectrochim. Acta Part B: Atom. Spectrosc.*, 63:367–374, 2008.

[15] R. Wester and R. Noll. Heuristic modeling of spectral plasma emission for laser-induced breakdown spectroscopy. *J. Appl. Phys.*, 106(12):123302, 2009.

[16] G. H. Cavalcanti, D. V. Teixeira, S. Legnaioli, G. Lorenzetti, L. Pardini, and V. Palleschi. One-point calibration for calibration-free laser-induced breakdown spectroscopy quantitative analysis. *Spectrochim. Acta Part B: Atom. Spectrosc.*, 87:51–56, 2013.

[17] R. Gaudiuso, M. Dell'Aglio, O. De Pascale, S. Loperfido, A. Mangone, and A. De Giacomo. Laser-induced breakdown spectroscopy of archaeological findings with calibration-free inverse method: Comparison with classical laser-induced breakdown spectroscopy and conventional techniques. *Anal. Chim. Acta*, 813:15–24, 2014.

[18] C. Aragón and J. A. Aguilera. Direct analysis of aluminum alloys by csigma laser-induced breakdown spectroscopy. *Anal. Chim. Acta*, 1009: 12–19, 2018.

[19] S. Wicklein, A. Sambri, S. Amoruso, X. Wang, R. Bruzzese, A. Koehl, and R. Dittmann. Pulsed laser ablation of complex oxides: The role of congruent ablation and preferential scattering for the film stoichiometry. *Appl. Phys. Lett.*, 101:131601 1–5, 2012.

[20] X. L. Mao, A. C. Ciocan, and R. E. Russo. Preferential vaporization during laser ablation inductively coupled plasma atomic emission spectroscopy. *Appl. Spectrosc.*, 52:913–918, 1998.

[21] J. Hermann, L. Mercadier, E. Mothe, G. Socol, and P. Alloncle. On the stoichiometry of mass transfer from solid to plasma during pulsed laser ablation of brass. *Spectrochim. Acta Part B: Atom. Spectrosc.*, 65:636–641, 2010.

[22] R. W. P. McWhirter. Ch. 5. In R. H. Huddlestone, editor, *Plasma Diagnostic Techniques*, pages 201–264. Academic, New York, 1965.

[23] G. Cristoforetti, A. De Giacomo, M. Dell'Aglio, S. Legnaioli, E. Tognoni, V. Palleschi, and N. Omenetto. Local thermodynamic equilibrium in laser-

induced breakdown spectroscopy: Beyond the McWhirter criterion. *Spectrochim. Acta Part B: Atom. Spectrosc.*, 65:86–95, 2010.

[24] J. Lam, V. Motto-Ros, D. Misiak, C. Dujardin, G. Ledoux, and D. Amans. Investigation of local thermodynamic equilibrium in laser-induced plasmas: Measurements of rotational and excitation temperatures at long time scales. *Spectrochim. Acta Part B: Atom. Spectrosc.*, 101:86–92, 2014.

[25] W. Lei, V. Motto-Ros, M. Boueri, Q. Ma, D. Zhang, L. Zheng, H. Zeng, and J. Yu. Time-resolved characterization of laser-induced plasma from fresh potatoes. *Spectrochim. Acta Part B: Atom. Spectrosc.*, 64:891–898, 2009.

[26] K. K. Herrera, E. Tognoni, N. Omenetto, B. W. Smith, and J. D. Winefordner. Semi-quantitative analysis of metal alloys, brass and soil samples by calibration-free laser-induced breakdown spectroscopy: recent results and considerations. *J. Anal. At. Spectrom.*, 24:413–425, 2009.

[27] G. Cristoforetti, E. Tognoni, and L. A. Gizzi. Thermodynamic equilibrium states in laser-induced plasmas: From the general case to laser-induced breakdown spectroscopy plasmas. *Spectrochim. Acta Part B: Atom. Spectrosc.*, 90:1–22, 2013.

[28] C. Gerhard, J. Hermann, L. Mercadier, L. Loewenthal, E. Axente, C. R. Luculescu, T. Sarnet, M. Sentis, and W. Viöl. Quantitative analyses of glass via laser-induced breakdown spectroscopy in argon. *Spectrochim. Acta Part B: Atom. Spectrosc.*, 101:32–45, 2014.

[29] J. Hermann, A. Lorusso, A. Perrone, F. Strafella, C. Dutouquet, and

B. Torralba. Simulation of emission spectra from nonuniform reactive laser-induced plasmas. *Phys. Rev. E*, 92:053103 1–15, 2015.

[30] G. Travaillé, O. Peyrusse, B. Bousquet, L. Canioni, K. Michel-Le Pierres, and S. Roy. Local thermodynamic equilibrium and related metrological issues involving collisional-radiative model in laser-induced aluminum plasmas. *Spectrochim. Acta Part B: Atom. Spectrosc.*, 64(10, SI):931–937, 2009.

[31] V. Morel, A. Bultel, I. Schneider, and C. Grisolia. State-to-state modeling of ultrashort laser-induced plasmas. *Spectrochim. Acta Part B: Atom. Spectrosc.*, 127:7–19, 2017.

[32] D. Grojo, J. Hermann, and A. Perrone. Plasma analyses during femtosecond laser ablation of Ti, Zr, and Hf. *J. Appl. Phys.*, 97(6):063306 1–9, 2005.

[33] J. Hermann, C. Gerhard, E. Axente, and C. Dutouquet. Comparative investigation of laser ablation plumes in air and argon by analysis of spectral line shapes: Insights on calibration-free laser-induced breakdown spectroscopy. *Spectrochim. Acta Part B: Atom. Spectrosc.*, pages 189–196, 2014.

[34] J. Hermann, D. Grojo, E. Axente, C. Gerhard, M. Burger, and V. Craciun. Ideal radiation source for plasma spectroscopy generated by laser ablation. *Phys. Rev. E*, 96:053210 1–6, 2017.

[35] E. Axente, J. Hermann, G. Socol, L. Mercadier, S. A. Beldjilali, M. Cirisan, C. R. Luculescu, C. Ristoscu, I. N. Mihailescu, and V. Craciun. Accurate analysis of indium-zinc oxide thin films via laser-induced breakdown spec-

troscopy based on plasma modeling. *J. Anal. At. Spectrom.*, 29:553–564, 2014.

[36] P.B. Hansen, S. Schrder, S. Kubitza, K. Rammelkamp, D.S. Vogt, and H.-W. Hbers. Modeling of time-resolved libs spectra obtained in martian atmospheric conditions with a stationary plasma approach. *Spectrochimica Acta Part B: Atomic Spectroscopy*, 178:106115, 2021.

[37] M. Hafeez, S. A. Abbasi, M. Rafique, R. Hayder, M. Sajid, J. Iqbal, N. Ahmad, and S. Shahida. Calibration-free laser-induced breakdown spectroscopic analysis of copper-rich mineral collected from the gilgit-baltistan region of pakistan. *Appl. Opt.*, 59:68–76, 2020.

[38] J. D. Pedarnig, P. Kolmhofer, N. Huber, B. Praher, J. Heitz, and R. Roessler. Element analysis of complex materials by calibration-free laser-induced breakdown spectroscopy. *Appl. Phys. A: Mat. Sci. Proc.*, 112:105–111, 2013.

[39] A. Taleb, V. Motto-Ros, M. J. Carru, E. Axente, V. Craciun, F. Pelascini, and J. Hermann. Measurement error due to self-absorption in calibration-free laser-induced breakdown spectroscopy. *Anal. Chim. Acta*, 1185: 339070 1–7, 2021.

[40] A. M. El Sherbini, T. M. El Sherbini, H. Hegazy, G. Cristoforetti, S. Legnaioli, V. Palleschi, L. Pardini, A. Salvetti, and E. Tognoni. Evaluation of self-absorption coefficients of aluminum emission lines in laser-induced breakdown spectroscopy measurements. *Spectrochim. Acta Part B: Atom. Spectrosc.*, 60:1573–1579, 2005.

[41] G. Cristoforetti and E. Tognoni. Calculation of elemental columnar den-

sity from self-absorbed lines in laser-induced breakdown spectroscopy: A resource for quantitative analysis. *Spectrochim. Acta Part B: Atom. Spectrosc.*, 79-80:63–71, 2013.

[42] J. Hou, L. Zhang, Y. Zhao, Z. Wang, Y. Zhang, W. Ma Weiguang L., Dong, W. Yin, L. Xiao, and S. Jia. Mechanisms and efficient elimination approaches of self-absorption in LIBS. *Plasma Sci. Technol.*, 21:034016 1–15, 2019.

[43] I. B. Gornushkin, T. Völker, and A. Y. Kazakov. Extension and investigation by numerical simulations of algorithm for calibration-free laser induced breakdown spectroscopy. *Spectrochim. Acta Part B: Atom. Spectrosc.*, 147:149–163, 2018.

[44] J. J. Maali and S. V. Shabanov. Error analysis in optimization problems relevant for calibration-free laser-induced breakdown spectroscopy. *J. Quant. Spectrosc. Radiat. Transf.*, 222:236–246, 2019.

[45] A. De Giacomo and J. Hermann. Laser-induced plasma emission: from atomic to molecular spectra. *J. Phys. D: Appl. Phys.*, 50:183002 1–17, 2017.

[46] X. Bai, V. Motto-Ros, W. Lei, L. Zheng, and J. Yu. Experimental determination of the temperature range of alo molecular emission in laser-induced aluminum plasma in air. *Spectrochim. Acta Part B: Atom. Spectrosc.*, 99: 193–200, 2014.

[47] C.-T. Chen, D. Banaru, T. Sarnet, and J. Hermann. Two-step procedure for trace element analysis in food via calibration-free laser-induced

breakdown spectroscopy. *Spectrochim. Acta Part B: Atom. Spectrosc.*, 150:77–85, 2018.

[48] Ya. B. Zel'dovich and Yu. P. Raizer. *Physics of Shock Waves and High Temperature Phenomena*. Academic, New York, 1966.

[49] J. Hermann and C. Dutouquet. Local thermal equilibrium plasma modeling for analyses of gas-phase reactions during reactive-laser ablation. *J. Appl. Phys.*, 91:10188–10193, 2002.

[50] W.L. Wiese. 10. Electric Arcs. In B. Bederson and W. L. Fite, editors, *Atomic and Electron Physics*, volume 7 of *Methods in Experimental Physics*, pages 307–353. Academic Press, 1968.

[51] W. Lochte-Holtgreven. 3. evaluation of plasma parameters. In W. Lochte-Holtgreven, editor, *Plasma Diagnostics*, volume 7 of *American Vacuum Society classics*, page 135. North Holland, 1968.

[52] J. Cooper. Plasma spectroscopy. *Rep. Prog. Phys.*, 29:35–130, 1966.

[53] L. D. Pietanza, G. Colonna, A. De Giacomo, and M. Capitelli. Kinetic processes for laser induced plasma diagnostic: A collisional-radiative model approach. *Spectrochim. Acta Part B: Atom. Spectrosc.*, 65:616–626, 2010.

[54] V. Morel, A. Bultel, and B. G. Cheron. Modeling of thermal and chemical non-equilibrium in a laser-induced aluminum plasma by means of a collisional-radiative model. *Spectrochim. Acta Part B: Atom. Spectrosc.*, 65(9-10):830–841, 2010.

[55] C. A. D'Angelo, D. M. Diaz Pace, and G. Bertuccelli. Semiempirical model for analysis of inhomogeneous optically thick laser-induced plasmas. *Spectrochim. Acta Part B: Atom. Spectrosc.*, 64:999–1008, 2009.

[56] S. V. Shabanov and I. B. Gornushkin. Geometrical effects in data collection and processing for calibration-free laser-induced breakdown spectroscopy. *J. Quant. Spectrosc. Radiat. Transf.*, 204:190–205, 2018.

[57] J. Hermann, E. Axente, F. Pelascini, and V. Craciun. Analysis of multielemental thin films via calibration-free laser-induced breakdown spectroscopy. *Anal. Chem.*, 91:2544–2550, 2019.

[58] C. Gerhard, A. Taleb, F. Pelascini, and J. Hermann. Quantification of surface contamination on optical glass via sensitivity-improved calibration-free laser-induced breakdown spectroscopy. *Appl. Surf. Sci.*, 537:147984 1–7, 2021.

[59] D. W. Hahn and N. Omenetto. Laser-induced breakdown spectroscopy (LIBS), Part II: Review of instrumental and methodological approaches to material analysis and applications to different fields. *Appl. Spectrosc.*, 66(4):347–419, 2012.

[60] T. E. Itina, J. Hermann, P. Delaporte, and M. Sentis. Laser-generated plasma plume expansion: Combined continuous-microscopic modeling. *Phys. Rev. E*, 66:066406, 2002.

[61] S. V. Shabanov and I. B. Gornushkin. Two-dimensional axisymmetric models of laser induced plasmas relevant to laser induced breakdown spectroscopy. *Spectrochim. Acta Part B: Atom. Spectrosc.*, 100:147–172, 2014.

[62] I. B. Gornushkin, A. Y. Kazakov, N. Omenetto, B. W. Smith, and J. D. Winefordner. Experimental verification of a radiative model of laser-induced plasma expanding into vacuum. *Spectrochim. Acta Part B: Atom. Spectrosc.*, 60:215–230, 2005.

[63] H. R. Griem. *Plasma spectroscopy.* Academic, New York, 1964.

[64] X. Z. Zhao, L. J. Shen, T. X. Lu, and K. Niemax. Spatial distributions of electron-density in microplasmas produced by laser ablation of solids. *Appl. Phys. B: Photophys. Laser Chem.*, 55:327–330, 1992.

[65] E. E. Whiting. An empirical approximation to voigt profile. *J. Quant. Spectrosc. Radiat. Transf.*, 8:1379–1384, 1968.

[66] J. Hermann, C. Shen, A. Hermann, O. Aleixo da Luz, A. Taleb, and F. Pelascini. Analyse élémentaire des matériaux sans étalonnage. *Photoniques*, 103:46–49, 2020.

[67] P. Yaroshchyk, D. Body, R. J. S. Morrison, and B. L. Chadwick. A semi-quantitative standard-less analysis method for laser-induced breakdown spectroscopy. *Spectrochim. Acta Part B: Atom. Spectrosc.*, 61(2):200–209, 2006.

[68] W. Q. Lei, J. El Haddad, V. Motto-Ros, N. Gilon-Delepine, A. Stankova, Q. Ma, X. S. Bai, L. J. Zheng, H. P. Zeng, and J. Yu. Comparative measurements of mineral elements in milk powders with laser-induced breakdown spectroscopy and inductively coupled plasma atomic emission spectroscopy. *Anal. Bioanal. Chem.*, 400:3303–3313, 2011.

[69] M. Dell'Aglio, A. De Giacomo, R. Gaudiuso, O. De Pascale, and S. Longo. Laser induced breakdown spectroscopy of meteorites as a probe of the early solar system. *Spectrochim. Acta Part B: Atom. Spectrosc.*, 101:68–75, 2014.

[70] R. Gaudiuso. Calibration-free inverse method for depth-profile analysis

with laser-induced breakdown spectroscopy. *Spectrochim. Acta Part B: Atom. Spectrosc.*, 123:105–113, 2016.

[71] Z. Q. Hao, L. Liu, R. Zhou, Y. W. Ma, X. Y. Li, L. B. Guo, Y. F. Lu, and X. Y. Zeng. One-point and multi-line calibration method in laser-induced breakdown spectroscopy. *Opt. Exp.*, 26(18):22926–22933, 2018.

[72] H. Shakeel, S. U. Haq, Q. Abbas, A. Nadeem, and V. Palleschi. Quantitative analysis of ge/si alloys using double-pulse calibration-free laser-induced breakdown spectroscopy. *Spectrochim. Acta Part B: Atom. Spectrosc.*, 146:101–105, 2018.

[73] N. Konjevic. Plasma broadening and shifting of non-hydrogenic spectral lines: Present status and applications. *Phys. Rep.*, 316:339–401, 1999.

[74] A. Safi, S. H. Tavassoli, G. Cristoforetti, E. Tognoni, B. Campanella, S. Legnaioli, S. Pagnotta, F. Poggialini, and V. Palleschi. Exploiting self-absorption for plasma characterization in laser-induced breakdown spectroscopy experiments: A comparison of two recent approaches. *Anal. Chem.*, 91:8595–8601, 2019.

[75] A. Taleb, C. Shen, D. Mory, K. Cieślik, S. Merk, M. R. Aziz, A. P. Caricato, C. Gerhard, F. Pelascini, and J. Hermann. Echelle spectrometer calibration by means of laser plasma. *Spectrochim. Acta Part B: Atom. Spectrosc.*, 178:106144, 2021.

[76] A. Elhassan, A. Giakoumaki, D. Anglos, G. M. Ingo, L. Robbiola, and M. A. Harith. Nanosecond and femtosecond laser induced breakdown spectroscopic analysis of bronze alloys. *Spectrochim. Acta Part B: Atom. Spectrosc.*, 63:504–511, 2008.

[77] L. Mercadier, J. Hermann, C. Grisolia, and A. Semerok. Plume segregation observed in hydrogen and deuterium containing plasmas produced by laser ablation of carbon fiber tiles from a fusion reactor. *Spectrochim. Acta Part B: Atom. Spectrosc.*, 65:715–720, 2010.

[78] A. Kramida, Y. Ralchenko, and J. Reader. NIST Atomic Spectra Database (version 5.8), 2020. URL http://physics.nist.gov/PhysRefData/ASD/. National Institute of Standards and Technology, Gaithersburg, MD.

[79] M. Cirisan, M. Cvejić, M. R. Gavrilović, S. Jovicević, N. Konjević, and J. Hermann. Stark broadening measurement of Al II lines in a laser-induced plasma. *J. Quant. Spectrosc. Radiat. Transfer*, 133:652–662, 2014.

[80] M. Burger and J. Hermann. Stark broadening measurements in plasmas produced by laser ablation of hydrogen containing compounds. *Spectrochim. Acta Part B: Atom. Spectrosc.*, 122:118–126, 2016.

[81] R. E. Russo, A. A. Bol'shakov, X. Mao, C. P. McKay, D. L. Perry, and O. Sorkhabi. Laser ablation molecular isotopic spectrometry. *Spectrochim. Acta Part B: Atom. Spectrosc.*, 66(2):99–104, 2011.